Structure and dynamics in a monolayer of dipolar spheres

Structure and dynamics in a monolayer of dipolar spheres

Peter D. Duncan and Philip J. Camp

Citation: J. Chem. Phys. **121**, 11322 (2004); doi: 10.1063/1.1812744
View online: http://dx.doi.org/10.1063/1.1812744
View Table of Contents: http://jcp.aip.org/resource/1/JCPSA6/v121/i22
Published by the AIP Publishing LLC.

Structure and dynamics in a monolayer of dipolar spheres

Peter D. Duncan and Philip J. Camp[a)]
School of Chemistry, University of Edinburgh, West Mains Road, Edinburgh EH9 3JJ, United Kingdom

(Received 28 May 2004; accepted 14 September 2004)

The structure and dynamics in a monolayer of dipolar soft spheres have been investigated using molecular dynamics simulations. This is a basic model of colloidal ferrofluid monolayers, and other magnetic liquids in planar geometries, which can exhibit self-assembled chainlike aggregates due to strong dipole-dipole interactions. The effects of such chaining on the structure, single-particle translational and rotational motions, and the collective rotational motions are examined. The signatures of aggregation in the various structural and dynamical functions considered in this study could prove useful in experimental investigations of strongly dipolar materials. © *2004 American Institute of Physics.* [DOI: 10.1063/1.1812744]

I. INTRODUCTION

The structure and phase behavior of strongly interacting dipolar fluids continues to attract attention from workers in various disciplines.[1] The most familiar examples of dipolar fluids are colloidal ferrofluids, consisting of roughly spherical ferromagnetic particles with diameters in the range 10 nm–1 μm dispersed in a simple solvent. The particles are usually coated with a thin layer of nonmagnetic inert material which prevents irreversible aggregation. The net interactions between the particles are mainly dipolar in nature, with the coatings providing only relatively weak short-range dispersion interactions.

These materials are of significant technological utility, because the rheological properties can be ''switched'' with applied magnetic fields. From a fundamental point of view, however, such materials are of interest because of the structural and dynamical complexity at the ''molecular'' level. One of the most striking structural characteristics of colloidal ferrofluids (even in the absence of applied magnetic fields) is the self-assembly of particles to form chains, arising from the ''nose-to-tail'' configuration favored by the dipolar forces. The earliest experimental evidence of clustering in colloidal ferrofluids was obtained from thin films using electron microscopy almost 40 years ago.[2] The experimental study of colloidal ferrofluids has recently been rejuvenated through the use of improved synthetic methods and high-resolution transmission electron microscopy.[3–5] The structural similarities between colloidal ferrofluids and a diverse range of materials, such as living polymers, micelles and microemulsions, and biological actin gels,[6] have recently stimulated significant new theories of defect formation and phase behavior.[7,8]

The nature of clustering in strongly dipolar *bulk* fluids has been studied at great length, both theoretically[9–13] and by computer simulation;[14–16] for a comprehensive review, see Ref. 1. In these studies, the dipolar particles are modeled as either hard or soft spheres carrying a central point dipole. The pair potential is given by

$$u(r)=u_{sr}(r)+\frac{\boldsymbol{\mu}_1\cdot\boldsymbol{\mu}_2}{r^3}-\frac{3(\boldsymbol{\mu}_1\cdot\mathbf{r})(\boldsymbol{\mu}_2\cdot\mathbf{r})}{r^5}, \tag{1}$$

where $u_{sr}(r)$ is a short-range isotropic repulsive potential, and the remaining terms represent the dipole-dipole interaction in which $\boldsymbol{\mu}_i$ is the dipole on particle i, $\mathbf{r}$ is the interparticle separation vector, and $r=|\mathbf{r}|$.

One observation which will be relevant to the present work is that the static structure factor $S(q)$ of strongly dipolar three-dimensional fluids exhibits a characteristic $1/q$ power-law scaling at low wave vectors.[16] This scaling arises from the presence of chainlike clusters with persistence lengths of the order of 10 sphere diameters. In principle, $S(q)$ is accessible to scattering experiments, and hence the $1/q$ scaling provides one experimental fingerprint of chain formation. With regard to the phase behavior of bulk dipolar fluids, we note in passing that the existence of a bulk fluid-fluid phase separation driven entirely by dipolar interactions is still an open question.[7,17,18]

Calculations on two-dimensional dipolar systems are more directly relevant to common experimental situations than are those on bulk systems, because the structural characterization of highly aggregated ferrofluids in experiments is largely carried out on thin films or on monolayers.[3–5] Monolayers of dipolar particles under more complex conditions—such as in static[19] or alternating applied fields[20,21]—look set to provide new avenues for research. The current technological interest in thin-film devices and functional materials supplies an additional motivation.

Recently, Weis and co-workers have used computer simulations and theory to survey and examine a large variety of structures formed by two-dimensional monolayers of strongly interacting dipolar spheres.[22–26] In Ref. 22 the dipole orientations are confined to a two-dimensional plane, whereas in Refs. 23–26 the dipoles are free to rotate in three dimensions. Not surprisingly, chain formation occurs in these quasi-two-dimensional systems, although it seems to persist over a higher concentration range than in three dimensions. This can be rationalized on the basis of an increased entropic penalty associated with clustering in higher dimensions. A diverse range of structures arises from the way in which the

[a)]Electronic mail: philip.camp@ed.ac.uk

chains ''fold-up;'' for instance, at high densities where the spheres are almost close packed, vortical orientational order appears. The characterization of chainlike clusters at low densities has been achieved by adapting equilibrium theories developed for bulk dipolar fluids.[24,25] In none of the studies cited above has there been any evidence of a fluid-fluid phase separation.

The discussion so far has been focused on the microstructural and thermodynamic properties of strongly dipolar fluids. Although the bulk hydrodynamic properties of magnetic fluids are well known,[27] the microscopic dynamics of strongly interacting dipolar particles appears to represent a rich area for further study. Wen *et al.* have carried out an interesting study of the aggregation kinetics of quasi-two-dimensional dipolar fluids[28] by conducting experiments with nickel-plated glass beads, and carrying out molecular dynamics (MD) computer simulations. They showed that the formation of chainlike clusters consisted of rapid association of small numbers of particles to form short chains, followed by the slow aggregation of these chains to form larger chains, and rings. This suggests that there will likely be at least two characteristic time scales present in the *equilibrium* dynamics, one representative of single-particle motion, and the other due to the collective motions of particles within a chain. This scenario has been demonstrated in MD and Brownian dynamics simulations of highly aggregated three-dimensional dipolar soft spheres.[29] The dielectric (or magnetic susceptibility) spectrum was seen to exhibit a high-frequency feature arising from the oscillations of single-dipole orientations within the chains, and a low-frequency feature arising from the relaxation of large aggregates.

In this work we examine the structure and dynamics of a model quasi-two-dimensional dipolar fluid using MD simulations. We consider a fluid comprising N dipolar soft spheres with mass m and moment of inertia I, confined to a two-dimensional square plane of area $A=L\times L$. The interparticle potential is given by Eq. (1) with the short-range part given by

$$u_{sr}(r)=4\epsilon\left(\frac{\sigma}{r}\right)^{12}, \tag{2}$$

where ϵ is an energy parameter and σ is the sphere ''diameter.'' It is emphasized that the dipoles are three-dimensional, and that they interact via the appropriate three-dimensional potential in Eq. (1). We employ reduced units for various molecular, thermodynamic, and dynamical quantities, defined as follows: density $\rho^*=N\sigma^2/A$; temperature $T^*=k_BT/\epsilon$, where k_B is Boltzmann's constant; dipole moment $\mu^*=\sqrt{\mu^2/\epsilon\sigma^3}$; moment of inertia $I^*=I/m\sigma^2$; and time $t^*=t\sqrt{\epsilon/m\sigma^2}$.

We confirm that at high dipole moments, the low-q behavior of $S(q)$ conforms to the same scaling law observed in three-dimensional dipolar fluids.[16] We investigate the translational and orientational dynamics of the two-dimensional system, paying particular attention to the characteristic properties of various time-correlation functions and their associated spectra. It is hoped that this work will provide useful experimental ''fingerprints'' for strong association in dipolar fluids.

This paper is organized as follows: In Sec. II we summarize the simulation methods used in this work. In Sec. III A we study the structure of the dipolar fluid, as represented by $S(q)$ and the corresponding radial distribution function $g(r)$. In Sec. III B, we present results for the single-particle diffusion coefficient and the velocity autocorrelation function, and assess the impact of chaining on these quantities. The single-particle rotational motion is studied in Sec. III C using the single-dipole autocorrelation function, and the single-particle angular velocity autocorrelation function. Collective rotational motions as evidenced by the bulk polarization autocorrelation functions are considered briefly in Sec. III D. Section IV concludes the paper.

II. MOLECULAR DYNAMICS COMPUTER SIMULATIONS

In all cases MD simulations were performed in the N-V-E ensemble after equilibration in the N-V-T ensemble at a temperature $T^*=1.0$ (achieved by translational and angular velocity scaling). We have used systems of $N=961$ particles with $m=1$ and $I^*=0.1$ throughout. The dipole orientations were represented using quaternions, and the dipolar interactions were handled using a spherical cutoff at $L/2$; the potential was truncated smoothly between $0.9\times L/2$ and $L/2$ using the switching function due to Andrea *et al.*[30] We justify our choice of a truncated potential (as opposed to calculating full Ewald sums) by reference to a recent study in which a cut-off $r_c>5\sigma$ was found to be sufficient to saturate the three-dimensional dipole-dipole interactions in two-dimensional arrays of particles.[31] For the system size simulated in this work, the cutoff is $r_c=L/2\geqslant 21.92\sigma$, the lower limit corresponding to the highest density ($\rho^*=0.5$) considered. The equations of motion were integrated using a velocity-Verlet algorithm for the translational motion, and a leapfrog algorithm for the rotational motion.[32] Simulations consisted of $O(10^5)$ time steps after equilibration, one time step being $\delta t^*=0.0025$. Periodic boundary conditions were applied. Typical simulation timings on a 1.3 GHz processor were 0.2 s per MD step. We have performed a series of N-V-E-MD simulations corresponding to a temperature $T^*=1.0$, and with various dipole moments ($\mu^*=0$, 0.5, 1, 1.5, 2, 2.5, and 2.75) and densities ($\rho^*=0.05$, 0.1, 0.2, 0.3, and 0.5).

III. RESULTS

A. Structure

Figure 1 shows some snapshots from simulations at the state points ($\mu^*=0.5,\rho^*=0.05$), ($\mu^*=0.5,\rho^*=0.5$), ($\mu^*=2.75,\rho^*=0.05$), and ($\mu^*=2.75,\rho^*=0.5$). With the lowest dipole moment ($\mu^*=0.5$) there is very little positional or orientational order apparent in the snapshots, whereas with the high dipole moment ($\mu^*=2.75$) the system is almost completely aggregated over the entire density range considered in this study ($0.05\leqslant\rho^*\leqslant 0.5$). In the aggregated regime, the particles are very strongly aligned in linear chains and rings, with the dipolar orientations adopting the nose-to-tail conformation. At all densities simulated in this work, the onset of aggregation occurs at $\mu^*>2$. This is illustrated in

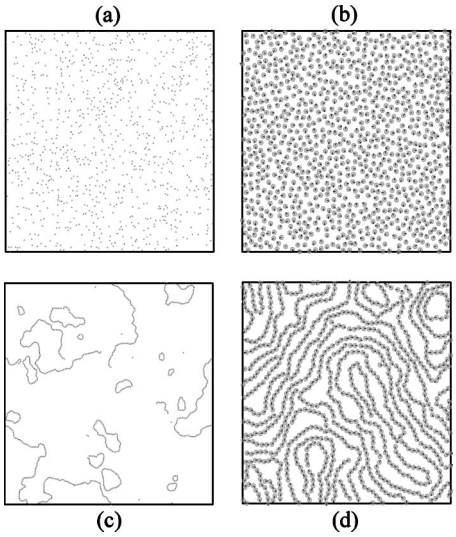

FIG. 1. Snapshots showing the positional and orientational ordering of the particles in systems with dipole moment μ^* and density ρ^*: (a) $\mu^*=0.5$, $\rho^*=0.05$; (b) $\mu^*=0.5$, $\rho^*=0.5$; (c) $\mu^*=2.75$, $\rho^*=0.05$; (d) $\mu^*=2.75$, $\rho^*=0.5$. The particles are represented by gray spheres with diameter σ, and the dipole orientations are shown as black lines of length 0.5σ emanating from the centers of the spheres.

Fig. 2 which shows snapshots from simulations at a fixed density of $\rho^*=0.2$. For dipole moments $\mu^*\leqslant 2$ the structure is quite uniform, although with $\mu^*=2$ there are a few relatively small and loosely clustered chainlike aggregates. Moving to higher dipole moments, however, results in a dramatic increase in the degree and extent of particle clustering.

In order to characterize the in-plane ordering of the particle centers of mass, the radial distribution function $g(r)$ was calculated in the usual way.[32] Some representative results are shown in Fig. 3 for weakly dipolar ($\mu^*=0.5$) and strongly dipolar ($\mu^*=2.75$) systems. At $\mu^*=0.5$ the structure is absolutely typical of a simple liquid, with peaks

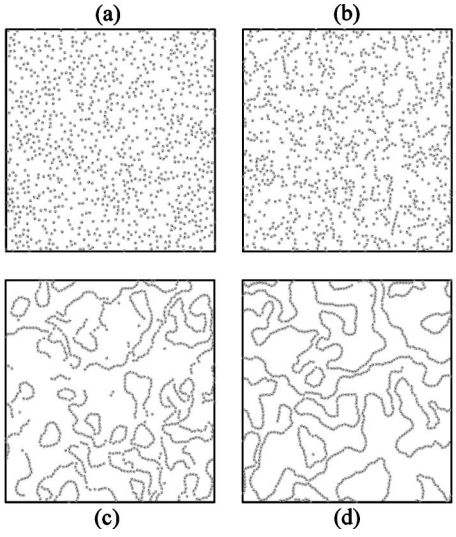

FIG. 2. Snapshots showing the positional and orientational ordering of the particles in systems with density $\rho^*=0.2$ and dipole moment μ^*: (a) $\mu^*=1.5$; (b) $\mu^*=2$; (c) $\mu^*=2.5$; (d) $\mu^*=2.75$. The particles are represented by gray spheres with diameter σ, and the dipole orientations are shown as black lines of length 0.5σ emanating from the centers of the spheres.

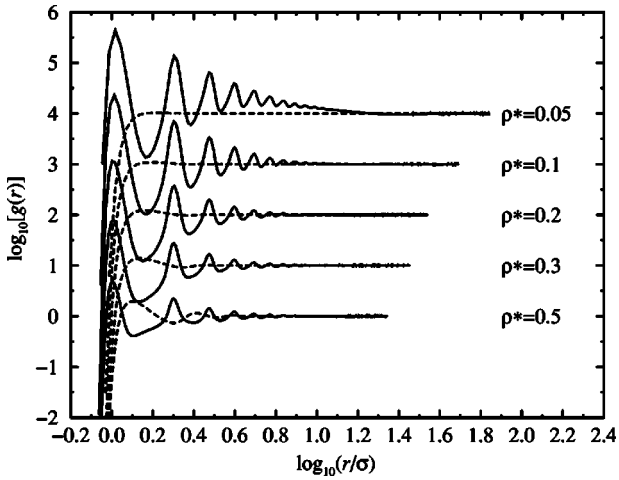

FIG. 3. Logarithms of the radial distribution functions $\log_{10}[g(r)]$ as functions of $\log_{10}(r/\sigma)$ from simulations with $\mu^*=0.5$ (dashed lines) and $\mu^*=2.75$ (solid lines), and at various densities in the range $0.05\leqslant\rho^*\leqslant 0.5$. The curves are displaced by one unit along the ordinate for clarity.

emerging at $r\simeq 1.2\sigma$ and $r\simeq 2.6\sigma$ with increasing density. In stark contrast, with the highest dipole moment ($\mu^*=2.75$) and at all densities, $g(r)$ shows pronounced peaks close to integer values of σ. This structure corresponds to chaining of the dipolar particles with the dipoles aligned ''nose to tail;'' the peaks shift to lower distances as the dipole moment is increased because of the strongly attractive interaction for dipoles in this orientation. To understand the position of the first peak in $g(r)$, we consider the minimum-energy configuration for pairs of dipoles interacting via the potential given by Eqs. (1) and (2). This configuration corresponds to the particles with dipoles parallel and colinear with the interparticle separation vector, i.e., $\boldsymbol{\mu}_1\cdot\boldsymbol{\mu}_2=\mu^2$, $\boldsymbol{\mu}_1\cdot\mathbf{r}=\boldsymbol{\mu}_2\cdot\mathbf{r}=\mu r$. The position and depth of the potential minimum are given by

$$r_0=2^{1/3}(\mu^*)^{-2/9}\sigma \tag{3}$$

and

$$u(r_0)=-\tfrac{3}{4}(\mu^*)^{8/3}\epsilon, \tag{4}$$

respectively. At $\mu^*=0.5$, the potential minimum occurs at $r_0=1.47\sigma$, whereas at $\mu^*=2.75$, $r_0=1.01\sigma$; these rough estimates are in accord with the positions of the first peak in $g(r)$ shown in Fig. 3.

To examine the fluid structure further, we computed the static structure factor $S(q)$ from the Fourier transform of $h(r)=g(r)-1$,[33]

$$S(q)=1+\int h(r)\exp(-i\mathbf{q}\cdot\mathbf{r})d\mathbf{r},$$

$$=1+2\pi\rho\int_0^\infty rJ_0(qr)h(r)dr, \tag{5}$$

where $J_0(z)$ is a Bessel function of the first kind. In Fig. 4 we present $S(q)$ for systems with $\mu^*=0.5$ and $\mu^*=2.75$ at densities in the range $0.05\leqslant\rho^*\leqslant 0.5$. In the weakly dipolar case, $S(q)$ looks absolutely typical for a simple fluid, whereas with $\mu^*=2.75$ it shows significant complexity. As

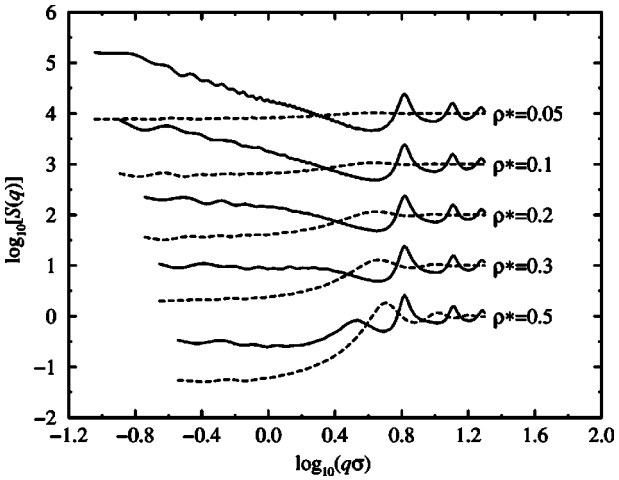

FIG. 4. Logarithms of the static structure factors $\log_{10}[S(q)]$ as functions of $\log_{10}(q\sigma)$ from simulations with $\mu^*=0.5$ (dashed lines) and $\mu^*=2.75$ (solid lines), and at various densities in the range $0.05\leqslant\rho^*\leqslant0.5$. The curves are displaced by one unit along the ordinate for clarity.

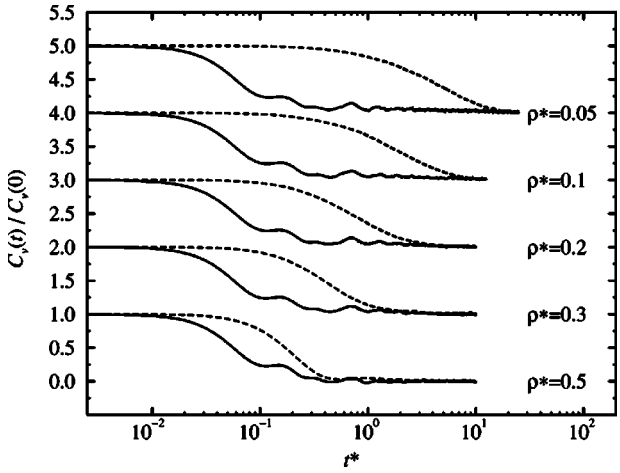

FIG. 5. Normalized velocity autocorrelation functions $C_v(t)/C_v(0)$ for systems with $\mu^*=0.5$ (dashed lines) and $\mu^*=2.75$ (solid lines), and at various densities in the range $0.05\leqslant\rho^*\leqslant0.5$. The curves for each density are displaced by one unit along the ordinate for clarity.

the dipole moment is increased, the peaks at $q\sigma>2.5=10^{0.40}$ shift to higher wave vectors, reflecting the decreased separation between near neighbors in the chains. At $\mu^*=2.75$ and $\rho^*=0.05$, $S(q)$ exhibits a power-law dependence on q in the range $q\sigma<4.0=10^{0.60}$; a fit to these results in the range $q\sigma<4.0$ shows that $S(q)\sim q^{-\alpha}$ with $\alpha=1.02\pm0.01$. This is in good agreement with the observed scaling of $S(q)$ for chainlike aggregates in three dimensions ($\alpha=1$),[16] confirming that this is a reliable signal for aggregation in dipolar fluids in both two and three dimensions. In general, this kind of scaling is only apparent with dipole moments $\mu^*>2$, suggesting that this inequality delineates a boundary between ''dissociated'' and ''associated'' regimes. This is in accordance with Fig. 2 and the dynamical evidence presented below. $S(q)$ for the most strongly dipolar and dense system ($\mu^*=2.75,\rho^*=0.5$) exhibits an interesting ''prepeak'' at $q\sigma\simeq3.4=10^{0.54}$, corresponding to a real-space distance of about $2\pi/q\simeq1.8\sigma$; this feature is due to the local parallel ordering of chain segments, as is shown in Fig. 1(d). To summarize, at the highest dipole moments the molecular-scale structure—as characterized by $g(r)$ and $S(q)$—is reminiscent of that observed in three-dimensional dipolar fluids.[16] In both two and three dimensions, the fluid at low densities and temperatures consists of ringlike and chainlike clusters formed from particles in the nose-to-tail configuration, leading to an apparent $1/q$ scaling in the structure factor.

B. Single-particle translational motion

We now turn to the single-particle translational motions in the dipolar fluid. We have calculated the velocity autocorrelation function $C_v(t)$ defined by

$$C_v(t)=\left\langle \frac{1}{N}\sum_{i=1}^{N}\mathbf{v}_i(t)\cdot\mathbf{v}_i(0)\right\rangle, \tag{6}$$

where $\mathbf{v}_i(t)$ is velocity of particle i at time t and the angled brackets denote an average over time origins. Some representative results are shown in Fig. 5 for systems with dipole moments $\mu^*=0.5$ and $\mu^*=2.75$. With a low dipole moment ($\mu^*=0.5$) $C_v(t)$ exhibits a decay typical of simple dilute fluids. At higher dipole moments, however, there is a significant modulation of the curves, and only very small negative portions at the highest densities. We interpret this as being another significant indication of particle chaining. Over short periods of time a tagged particle within a chain can oscillate about its ''equilibrium'' position between its two nearest neighbors, which might be expected to give rise to oscillatory behavior in $C_v(t)$. The chain as whole is also moving, however, and so any given tagged particle will also have a ''drift'' velocity which is then modulated by its local motions within the chain. This scenario seems consistent with the results for $\mu^*=2.75$ presented in Fig. 5.

It is well known that in simple two-dimensional fluids, hydrodynamic modes can give rise to a t^{-1} ''long-time tail'' in $C_v(t)$.[33,34] From the Green-Kubo relation

$$D=\frac{1}{2}\int_0^\infty C_v(t)dt, \tag{7}$$

this long-time tail should lead to a divergent diffusion constant D. Simulation studies of soft-sphere fluids[35] have shown that at high densities ($\rho^*>0.9$) such hydrodynamic effects are absent. In the present case, the highly clustered structures of fluids with high dipole moments might mitigate against the hydrodynamic backflow that gives rise to the long-time tail in $C_v(t)$. Although we cannot categorically rule out the presence of long-time tails, in practice no such features were apparent in $C_v(t)$ within the statistical noise. With this in mind, we have calculated *estimates* of D using Eq. (7), and by computing the mean squared displacement,

$$\Delta R^2(t)=\left\langle \frac{1}{N}\sum_{i=1}^{N}|\mathbf{r}_i(t)-\mathbf{r}_i(0)|^2\right\rangle, \tag{8}$$

where the angled brackets denote an average over time origins. In calculating $\Delta R^2(t)$ we allow the particles to diffuse out of the central simulation cell. As far as we could tell from finite-length simulations, for all of the systems considered in

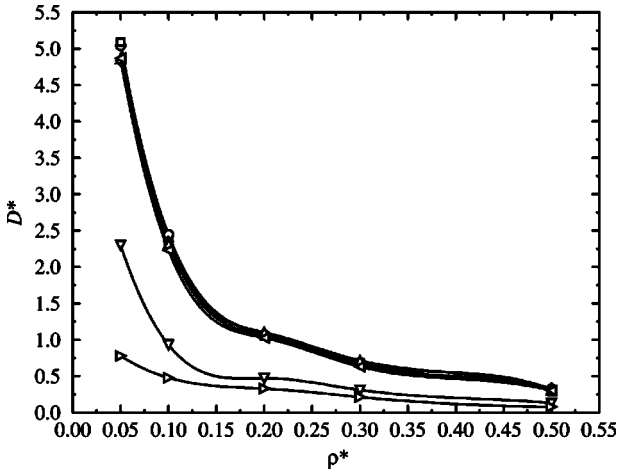

FIG. 6. Reduced diffusion coefficient (see text) as a function of density ρ^* at various dipole moments: $\mu^*=0$ (circles); $\mu^*=0.5$ (squares); $\mu^*=1$ (diamonds); $\mu^*=1.5$ (up triangles); $\mu^*=2$ (left triangles); $\mu^*=2.5$ (down triangles); $\mu^*=2.75$ (right triangles). The solid lines are cubic spline fits to guide the eye. Note that the curves for $0\leqslant\mu^*\leqslant 2$ are almost coincident.

this work $\Delta R^2(t)$ exhibited an approximately linear asymptotic dependence on time. If ΔR^2 exhibits a linear dependence on time at long times, then the diffusion constant D can be defined in two dimensions by the Einstein relation

$$\Delta R^2(t)=4Dt. \tag{9}$$

We found that the values for D obtained from Eqs. (7) and (9) agreed with one another to within 1%. Although it is likely that hydrodynamic effects operate in some of the systems considered in this work, their impact on the measured values of D appears to be small. Nonetheless, the values of D obtained here provide some sort of measure of the single-particle diffusion. In Fig. 6 we plot the reduced diffusion coefficient, $D^*=D\sqrt{m/\epsilon\sigma^2}$, as a function of density for systems with dipole moments in the range $0.5\leqslant\mu^*\leqslant 2.75$. The first thing to note is that the diffusion coefficient decreases with increasing density, as expected. The variation with dipole moment at fixed density is more illuminating. For dipole moments $\mu^*\leqslant 2$, the curves are almost coincident suggesting that the dipolar interactions in this regime have very little effect on the single-particle motion. For dipole moments $\mu^*\geqslant 2.5$, however, the curves are displaced downwards. Essentially the particles become trapped in clusters for long times with the effect of increasing the time scales for single-particle diffusion. The onset of strong association for $\mu^*>2$ evidenced by these dynamical results is consistent with that observed in simulation snapshots and the structural quantities described in Sec. III A. For reference, the values of the diffusion constant are listed in Table I.

C. Single-particle rotational motion

To investigate the impact of chaining upon single-particle rotational motion, we have calculated single-dipole orientation autocorrelation functions defined by

$$C_\mu^\alpha(t)=\left\langle \frac{1}{N\mu^2}\sum_{i=1}^{N}\mu_i^\alpha(t)\mu_i^\alpha(0)\right\rangle, \tag{10}$$

where $\alpha=x$, y, z, and μ_i^α is the component of the dipole vector on particle i along the α axis of the laboratory frame. The function $C_\mu^{xy}(t)=[C_\mu^x(t)+C_\mu^y(t)]$ will therefore characterize the rotational motions of dipoles within the plane of the monolayer, whereas $C_\mu^z(t)$ will reflect out-of-plane motions. In Fig. 7 we compare results for two systems at a density $\rho^*=0.5$ and with dipole moments $\mu^*=0.5$ and $\mu^*=2.75$. With the lower dipole moment ($\mu^*=0.5$) both in-plane and out-of-plane functions show damped oscillatory behavior due to weakly hindered rotations of the dipoles. The quantities $C_\mu^{xy}(0)=0.67$ and $C_\mu^z(0)=0.33$ show that there is no preferred direction of alignment (either in plane or out of plane) for the dipoles at this state point. The weak dipolar forces are therefore insignificant, and so it is anticipated that the reorientational angular frequency in this system will be close to the free-rotor limit, $\omega_0^*=\sqrt{T^*/I^*}=\sqrt{10}$; this is confirmed below. With the higher dipole moment ($\mu^*=2.75$) the in-plane and out-of-plane functions are very different. First, the quantities $C_\mu^{xy}(0)=0.966$ and $C_\mu^z(0)=0.034$ confirm that the dipoles are strongly constrained to lie within the plane. Second, at this admittedly quite extreme dipole moment, $C_\mu^{xy}(t)$ is seen to decay only very slowly but with a small oscillatory modulation. This is clearly a consequence of rapid single-dipole oscillations about the equilibrium nose-to-tail orientations within the chain, while the chain as a whole is rotating only very slowly. The separation between time scales for single-particle and chain rotational motions is analogous to that observed for single-particle and chain translations apparent in the velocity autocorrelation functions discussed in Sec. III B. The out-of-plane function $C_\mu^z(t)$ shows a clear damped oscillation about zero. In Table I we present the values of $C_\mu^z(0)$ for all of the systems considered in this work. $C_\mu^z(0)$ reflects a sharp change in orientational structure that occurs between $\mu^*=2$ and $\mu^*=2.5$. With $\mu^*\leqslant 2$ the values of $C_\mu^z(0)$ are only weakly dependent on density, and for the most part are in close agreement with the value for random dipolar orientations [$C_\mu^z(0)=1/3$]. With $\mu^*=2.5$ and $\mu^*=2.75$ the values of $C_\mu^z(0)$ are very much smaller, reflecting the preferential alignment of dipoles within the plane.

In principle, the time scales for oscillatory orientational motions within the plane and perpendicular to the plane may differ as a result of interchain forces. However, even at the highest density ($\rho^*=0.5$) the mean separation between the chains is significant [see Fig. 1(d)] which suggests that $C_\mu^{xy}(t)$ and $C_\mu^z(t)$ will exhibit similar periods of oscillation. To this end, we have examined the Fourier transforms of $C_\mu^{xy}(t)$ and $C_\mu^z(t)$. Clearly the decay time of $C_\mu^{xy}(t)$ for the system with $\mu^*=2.75$ and $\rho^*=0.5$—as shown in Fig. 7—is very much longer than the duration of the simulation, precluding an accurate calculation of its Fourier transform. Nonetheless, if we use a windowing function, the high-frequency oscillation should still give rise to some sort of peak in the Fourier transform. This extreme truncation will give rise to pathological low-frequency features in the spectrum, but the high-frequency region—where we expect the single-dipole oscillations to manifest themselves—should emerge relatively unscathed. Obviously, calculation of the the Fourier transform of $C_\mu^z(t)$ presents no such problems,

TABLE I. Dynamical properties of the quasi-two-dimensional dipolar fluid: reduced translational diffusion constant $D^*=D\sqrt{m/\epsilon\sigma^2}$; reduced rotational diffusion constant $D_R^*=D_R\sqrt{m\sigma^2/\epsilon}$; single-dipole orientation autocorrelation function at $t=0$, $C_\mu^z(0)$; autocorrelation functions at $t=0$ for the in-plane polarization, $C_P^{xy}(0)$, and the out-of-plane polarization, $C_P^z(0)$; reduced characteristic angular frequencies ω_0^* for single-particle rotational motion estimated from the Fourier transforms of $C_\mu^z(t)$ and $C_\Omega(t)$, and from the approximate theoretical expression in Eq. (15).

							ω_0^*		
μ^*	ρ^*	D^*	D_R^*	$C_\mu^z(0)$	$C_P^{xy}(0)$	$C_P^z(0)$	From $C_\mu^z(t)$	From $C_\Omega(t)$	Eq. (15)
0.5	0.05	5.1		0.33	0.67	0.32	3.6		1.9
	0.1	2.3		0.34	0.67	0.33	3.5		1.9
	0.2	1.1		0.33	0.71	0.30	3.6		1.9
	0.3	0.69		0.34	0.72	0.30	3.5		1.9
	0.5	0.29		0.33	0.74	0.26	3.5		1.9
1	0.05	4.8		0.33	0.68	0.30	3.6		4.9
	0.1	2.4		0.33	0.71	0.27	3.6		4.9
	0.2	1.1		0.33	0.83	0.21	3.7		4.9
	0.3	0.66		0.32	0.97	0.21	3.8		4.9
	0.5	0.34		0.31	1.3	0.17	4.2		4.9
1.5	0.05	4.9	133	0.33	0.71	0.26	3.7		8.4
	0.1	2.3	56	0.32	0.85	0.22	3.9		8.4
	0.2	1.1	27	0.30	1.1	0.16	4.2		8.4
	0.3	0.71	13	0.28	1.4	0.14	4.5		8.4
	0.5	0.31	5.2	0.23	2.1	0.082	5.2		8.4
2	0.05	4.9	58	0.29	0.95	0.20	4.0		12.4
	0.1	2.2	21	0.25	1.4	0.17	4.7		12.4
	0.2	1.0	6.9	0.20	2.2	0.10	5.5	6.4	12.4
	0.3	0.63	3.4	0.17	2.3	0.067	6.4	7.7	12.4
	0.5	0.30	1.4	0.13	2.8	0.049	7.6	8.3	12.4
2.5	0.05	2.3	18	0.082	6.7	0.055	10.3	12.2	16.6
	0.1	0.93	4.8	0.068	11	0.043	12.4	12.2	16.6
	0.2	0.47	1.3	0.057	8.5	0.034	12.7	12.3	16.6
	0.3	0.31	0.74	0.057	2.2	0.028	12.5	12.4	16.6
	0.5	0.13	0.34	0.052	3.3	0.022	12.7	12.4	16.6
2.75	0.05	0.78	1.9	0.035	11	0.023	14.0	14.2	18.9
	0.1	0.48	0.83	0.036	15	0.021	14.3	14.3	18.9
	0.2	0.33	0.34	0.035	111	0.023	14.6	14.3	18.9
	0.3	0.21	0.22	0.035	250	0.019	14.6	14.3	18.9
	0.5	0.079	0.19	0.034	280	0.016	14.3	14.5	18.9

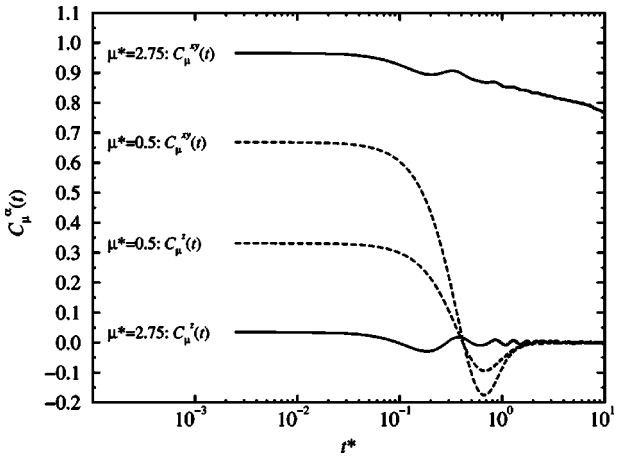

FIG. 7. Single-dipole autocorrelation functions $C_\mu^{xy}(t)=[C_\mu^x(t)+C_\mu^y(t)]$ and $C_\mu^z(t)$ for systems at a density of $\rho^*=0.5$, and with dipole moments $\mu^*=0.5$ (dashed lines) and $\mu^*=2.75$ (solid lines).

but nonetheless we have applied a Blackman windowing function throughout.[32] For the system with $\mu^*=2.75$ and $\rho^*=0.5$ we find peaks in the Fourier transforms of both $C_\mu^{xy}(t)$ and $C_\mu^z(t)$ at a characteristic reduced angular frequency of $\omega_0^*=14.3$. The conclusion is that even at this high density and dipole moment—at which interchain interactions might be significant—the estimates of reorientational time scales extracted from $C_\mu^{xy}(t)$ and $C_\mu^z(t)$ are essentially the same. In the following we therefore concentrate on $C_\mu^z(t)$ since it is easier to calculate Fourier transforms reliably.[36] To assist in comparisons, we present the function

$$\chi_\mu^z(\omega)=\frac{1}{2\pi C_\mu^z(0)}\int_{-\infty}^{\infty}C_\mu^z(t)\exp(-i\omega t)dt, \tag{11}$$

which is simply the Fourier transform of $C_\mu^z(t)$ normalized to unit area. Figure 8 shows $\chi_\mu^z(\omega)$ for systems at a density

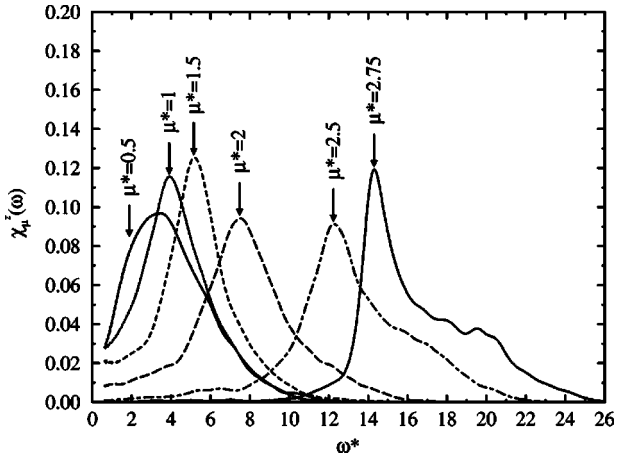

FIG. 8. Normalized Fourier transform of the z component of the single-dipole autocorrelation function $\chi_\mu^z(\omega)$ for systems at a density of $\rho^*=0.5$, and with dipole moments in the range $0.5\leqslant\mu^*\leqslant2.75$.

$\rho^*=0.5$ and dipole moments in the range $0.5\leqslant\mu^*\leqslant2.75$. At the lowest dipole moment ($\mu^*=0.5$) the peak in $\chi_\mu^z(\omega)$ is centered at approximately $\omega_0^*=3.5$, which is close to the free-rotor limit $\omega_0^*=\sqrt{T^*/I^*}\simeq3.16$. The position of this primary peak in $\chi_\mu^z(\omega)$ shifts to higher frequency with increasing dipole moment, reflecting stronger interactions and the presence of chaining which contrive to align dipoles in a ''head-to-tail'' conformation with their nearest neighbors. It is also clear that with increasing dipole moment a pronounced high-frequency shoulder develops. We speculate that this feature is due to coupling between single-dipole orientational motions and collective rotational motions. We return to this point briefly in Sec. III D, but first we report the positions of the primary peaks in $\chi_\mu^z(\omega)$. We have fitted single Lorentzian functions to the spectra in the vicinity of the peaks to extract estimates of the peak positions; the results are shown in Table I. We note that at the highest dipole moments ($\mu^*=2.5$ and $\mu^*=2.75$) ω_0 is almost independent of density, reflecting the fact that chains are present over the whole density range considered, and that interchain interactions (which would be more significant at higher densities) are actually very weak. Given this observation, we provide simple theoretical estimates of the variation of ω_0 with dipole moment in the high-dipole-moment regime.

In the highly-chained regime it is reasonable to think of the rotational motion of a single dipole in a cluster as being quasiharmonic in that its orientation oscillates about its equilibrium position within the chain. Consider a tagged dipolar sphere as part of a perfectly straight chain oriented along the laboratory x axis in which all of the dipole moments (except the tagged dipole moment) are constrained parallel with the x axis. The equilibrium nearest-neighbor separation is r_0 [Eq. (3)], and for simplicity we consider the motion of the tagged dipole in the xy plane; as shown above, it does not matter in which plane we consider the motion because the effects of interchain interactions are weak. If the tagged dipole is given by $\boldsymbol{\mu}(t)=\mu[\cos\gamma(t),\sin\gamma(t),0]$—where γ is the angle subtended by the dipole moment and the x axis—then the resulting torque due to the rest of the dipoles is oriented along the z axis and has magnitude

$$2\sum_{n=1}^{\infty}\left[-\frac{2\mu^2\sin\gamma}{(nr_0)^3}\right]=-\frac{4\mu^2\zeta(3)}{r_0^3}\sin\gamma, \tag{12}$$

where $\zeta(3)\simeq1.202$ is the Riemann ζ function. For high dipole moments the deviation from perfect alignment will be small, and hence $\sin\gamma\approx\gamma$. In this limit the equation of motion is $\ddot{\gamma}=-\omega_0^2\gamma$ where ω_0 is given by

$$\omega_0=\sqrt{\frac{4\mu^2\zeta(3)}{Ir_0^3}}. \tag{13}$$

The equation of motion yields an oscillatory solution $\gamma(t)=\gamma(0)\cos\omega_0t+(\dot{\gamma}(0)/\omega_0)\sin\omega_0t$. The orientation autocorrelation function in the absence of damping (friction) is therefore proportional to

$$\langle\boldsymbol{\mu}(t)\cdot\boldsymbol{\mu}(0)\rangle\propto1-\langle\gamma^2\rangle+\langle\gamma^2\rangle\cos\omega_0t \tag{14}$$

and even with damping through rotational friction a peak should be apparent in the Fourier transform at an angular frequency given by Eq. (13). In Table I, a comparison is made between the peak positions obtained from simulations, and the result of combining Eqs. (3) and (13) which yields, in reduced units,

$$\omega_0^*=\sqrt{\frac{2(\mu^*)^{8/3}\zeta(3)}{I^*}}. \tag{15}$$

By construction Eq. (15) is consistent with the observation that ω_0^* is roughly independent of density at the highest dipole moments, but it overestimates the simulation results for systems with the highest dipole moments—$\mu^*=2.5$ and $\mu^*=2.75$—by about 30%. It is easy to understand why Eq. (15) yields an overestimate: this approximation is based on a perfectly linear rigid chain, with no account taken of thermal fluctuations in the shape and extent of the chain. These effects will reduce in magnitude the average field experienced by—and hence the ''vibrational'' frequency of—any given dipole within the chain.

We have measured the single-particle autocorrelation function of the angular velocity $\boldsymbol{\Omega}$ given by

$$C_\Omega(t)=\left\langle\frac{1}{N}\sum_{i=1}^{N}\boldsymbol{\Omega}_i(t)\cdot\boldsymbol{\Omega}_i(0)\right\rangle, \tag{16}$$

and performed a similar analysis to that carried out on $C_\mu^\alpha(t)$ above. As defined, $C_\Omega(0)=2k_BT/I$. Unsurprisingly we find the same general behavior as with $C_\mu^\alpha(t)$, including the shapes and positions of the peaks in the Fourier transforms; for completeness, in Table I we have included estimates of ω_0^* obtained from these peak positions. The estimates of ω_0^* obtained from $C_\Omega(t)$ and $C_\mu^z(t)$ are consistent, as expected. In Fig. 9 we show some examples of $C_\Omega(t)$ from simulations at a density of $\rho^*=0.5$ and dipole moments in the range $0.5\leqslant\mu^*\leqslant2.75$. With low dipole moments ($\mu^*\leqslant1$) the relaxation of this function occurs very slowly, and at long times monotonically, reflecting the lack of strong interparticle interactions. With increasing dipole moment $C_\Omega(t)$ develops oscillations which can be identified with the quasiharmonic motion described above.

From $C_\Omega(t)$ we have calculated the rotational diffusion constant D_R given by[33]

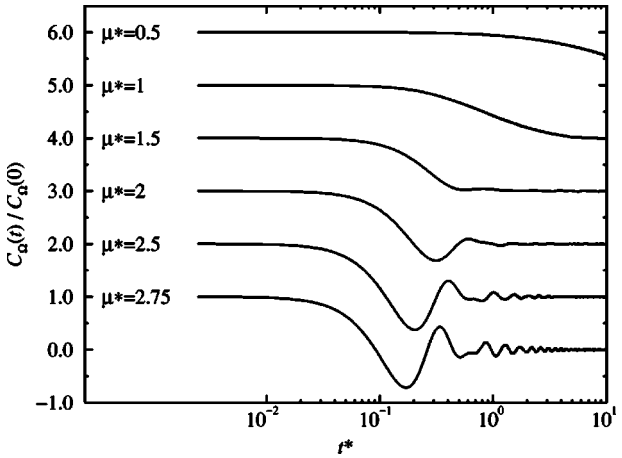

FIG. 9. Normalized angular velocity autocorrelation functions $C_\Omega(t)/C_\Omega(0)$ for systems at $\rho^*=0.5$ with various dipole moments in the range $0.5\leqslant\mu^*\leqslant 2.75$. The curves for each dipole moment are displaced by one unit along the ordinate for clarity.

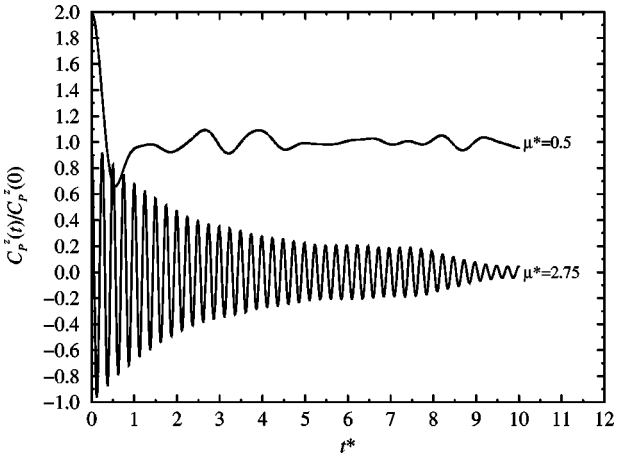

FIG. 10. Normalized autocorrelation function of the z component of the bulk polarization $C_P^z(t)/C_P^z(0)$ for systems at a density $\rho^*=0.5$ and dipole moments $\mu^*=0.5$ (top) and $\mu^*=2.75$ (bottom). The curves are displaced by one unit along the ordinate for clarity.

$$D_R=\tfrac{1}{2}\int_0^\infty C_\Omega(t)dt. \tag{17}$$

Some results are shown in Table I. The calculation of D_R was not possible at low dipole moments and low densities due to the very long decay of $C_\Omega(t)$ (see Fig. 9). For a given dipole moment, D_R decreases with increasing concentration; at high dipole moments this trend probably reflects an increased restriction of chain motions, as well as the quasiharmonic motions of single dipoles. For a given density D_R decreases with increasing dipole moment obviously due to increased aggregation.

D. Collective rotational motion

The problems encountered above with performing the Fourier transforms of single-dipole orientation autocorrelation functions are exacerbated when we turn to the analysis of the collective rotational motion. For exactly the same reasons as noted in Sec. III C, we will concentrate primarily on the autocorrelation function of the z component of the bulk polarization, rather than the x and y components. The bulk polarization is given by

$$\mathbf{P}(t)=\sum_{i=1}^{N}\boldsymbol{\mu}_i(t). \tag{18}$$

We define an autocorrelation function of its α component by

$$C_P^\alpha(t)=\frac{\langle P_\alpha(t)P_\alpha(0)\rangle}{N\mu^2}. \tag{19}$$

The function characterizing the in-plane polarization is $C_P^{xy}(t)=[C_P^x(t)+C_P^y(t)]$. At high dipole moments this function decays extremely slowly, with a decay time orders of magnitude larger than the length of our simulations; in some cases it hardly varies at all over simulation runs of $O(10^5)$ MD time steps. This situation appears analogous to the predicted increase of the Debye relaxation time in three-dimensional dipolar fluids as the dipole moment is increased.[37] A full analysis of $C_P^{xy}(t)$ is impractical, although the values of these functions at $t=0$ provide some measure of the in-plane susceptibility, this being proportional to $\langle P_x^2+P_y^2\rangle$. Values of $C_P^{xy}(0)$ are presented in Table I; these results show that the in-plane susceptibility increases markedly with increasing dipole moment [note that the trivial factor of μ^2 in the susceptibility is canceled in Eq. (19)]. This is due to the presence of long, almost linear segments within the chains which would be easily polarized with the application of an external field.

The autocorrelation function of the z component of the bulk polarization yields more information. For the purposes of illustration, we show $C_P^z(t)/C_P^z(0)$ in Fig. 10 for two systems at a density $\rho^*=0.5$, and with dipole moments $\mu^*=0.5$ and $\mu^*=2.75$. $C_P^z(t)$ exhibits damped oscillatory behavior in both cases, but clearly at high dipole moments the oscillation is of higher frequency and far less damped; crudely fitting a function of the form $C_P^z(t)\propto\exp(-t/\tau)\cos\omega_0 t$ in the range $0\leqslant t^*\leqslant 10$ yields $\tau\simeq 0.5$ and $\omega_0\simeq 5$ for $\mu^*=0.5$, and $\tau\simeq 3$ and $\omega_0\simeq 25$ for $\mu^*=2.75$. The value of $C_P^z(0)$ is proportional to the out-of-plane susceptibility and is shown in Table I. The results show that the out-of-plane susceptibility decreases with increasing dipole moment due to the preferred in-plane orientations of the dipoles.

We now turn to the Fourier transform of $C_P^z(t)$, which for the purposes of comparison is defined as a normalized quantity, i.e.,

$$\chi_P^z(\omega)=\frac{1}{2\pi C_P^z(0)}\int_{-\infty}^{\infty}C_P^z(t)\exp(-i\omega t)dt. \tag{20}$$

Figure 11 shows $\chi_P^z(\omega)$ for systems with density $\rho^*=0.5$ and dipole moments in the range $1.5\leqslant\mu^*\leqslant 2.75$; results for lower dipole moments are omitted for clarity as they consist of increasingly broad and noisy peaks. As in the case of single-particle rotational motion, the characteristic frequency increases with increasing dipole moment. For the systems with $\mu^*=2.5$ and $\mu^*=2.75$, the peaks in $\chi_P^z(\omega)$ are very sharp and well defined. In both cases, the positions of these peaks coincide with the high-frequency edge of the shoulder

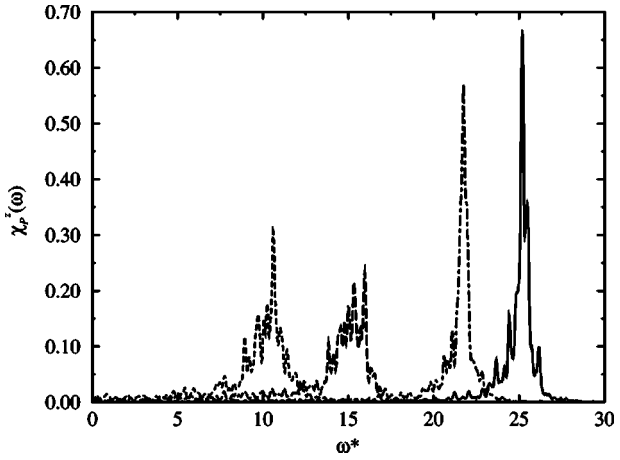

FIG. 11. Normalized Fourier transforms of the z component of the bulk polarization autocorrelation function $\chi_P^z(\omega)$ for systems at a density of $\rho^* = 0.5$, and with dipole moments in the range $1.5 \leqslant \mu^* \leqslant 2.75$. From left to right: $\mu^* = 1.5$ (short-dashed line); $\mu^* = 2$ (long-dashed line); $\mu^* = 2.5$ (dot-dashed line); $\mu^* = 2.75$ (solid line).

in the corresponding single-particle functions, $\chi_\mu^z(\omega)$. We suggest that this is a signal of some sort of coupling between single-particle and collective motions which give rise to the high-frequency shoulder in $\chi_\mu^z(\omega)$.

It is reasonable to suggest that long-range dipolar forces can lead to collective orientational motions within chains over considerable length scales. A full examination of these properties will require the calculation of space- and time-dependent correlation functions,[37] like $\langle \mathbf{P}(\mathbf{q},t)\cdot\mathbf{P}(-\mathbf{q},0)\rangle$, where $\mathbf{P}(\mathbf{q},t) = \Sigma_{j=1}^N \boldsymbol{\mu}_j(t)\exp[-i\mathbf{q}\cdot\mathbf{r}_j(t)]$ is a Fourier component of the bulk polarization. In the case of strongly chained systems at high dipole moments, this could lead to the identification of excitations analogous to spin waves in solid magnetic materials. In Refs. 37 and 38 relationships are derived between the single-particle relaxation time, $\tau = 1/2D_R$, associated with the decay of $\langle \boldsymbol{\mu}_i(t)\cdot\boldsymbol{\mu}_i(0)\rangle$, and the Debye relaxation time τ_D associated with the decay of $\langle \mathbf{P}(t)\cdot\mathbf{P}(0)\rangle$. In Ref. 38, for instance, the results are based on a micro-macro theorem stating that if the single-dipole correlation function can be expressed as a sum of decaying exponentials, then so can the bulk polarization correlation function. It is not clear whether such theories can be applied successfully to the very high dipole moment regime where the correlation functions are highly oscillatory; in the current work we have been concerned with oscillation frequencies in the correlation functions, not the decay times. To study the latter, accessing the relevant time scales will require much longer simulations than those conducted here, particularly for the in-plane motions.

IV. CONCLUSIONS

In this work, MD simulations have been used to study a simple model of fluid monolayers comprising spherical dipolar particles. Experimental realizations of these systems include colloidal ferrofluids and other magnetic liquids. The emphasis of this study has been on the effects of strong dipolar interactions on structure, and translational and orientational dynamics; these interactions favor the formation of chainlike aggregates, which profoundly affect the observable properties of the bulk material.

The signature of chaining on the structure factor has been examined, leading to the identification of power-law scaling at low wave vectors, analogous to that observed in simulations of three-dimensional dipolar fluids. This should provide a very clear fingerprint of chainlike aggregates which should be accessible in scattering experiments.

Dramatic effects of aggregation on the diffusion constant and the velocity autocorrelation function have been demonstrated. With weak dipolar interactions these quantities are absolutely typical for a simple two-dimensional ''atomic'' fluid. At high dipole moments, however, the chainlike aggregates lead to a discrimination between local ''intracluster'' motions and motions of clusters as integral units. The effect of the coupling between single-particle and collective motions is clearly visible in the velocity autocorrelation function. Unsurprisingly, aggregation is accompanied by a sharp drop in the single-particle diffusion coefficient, reflecting the fact that individual particles are strongly constrained by their nearest neighbors within the chain.

The orientational motion has been examined, and characteristic frequencies have been identified with particular types of motions. The characteristic frequencies for single-particle orientational motion have been determined from the Fourier transforms of the appropriate autocorrelation functions. At low dipole moments, the characteristic rotational frequency is close to the free-rotor limit. At high dipole moments this frequency is dictated by quasiharmonic oscillations of single-dipole orientations about the equilibrium orientations within chains, and hence the frequency increases with increasing dipole moment. In general, the characteristic frequencies are independent of density which implies that the interactions between neighboring chains are weak; moreover, we did not detect any distinction between the time scales for in-plane and out-of-plane rotational motions. A simple analysis of the effective field experienced by a tagged dipolar particle yields estimates of the characteristic frequencies accurate to within about 30% at high dipole moments. The Fourier transforms of the single-dipole orientation autocorrelation functions develop high-frequency shoulders with increasing dipole moment, which we suggest are due to the coupling between single-particle and collective motions. We have made a brief investigation of the collective rotational motions, the results of which are consistent with this hypothesis.

Further work is required, particularly in calculating space- and time-dependent correlation functions, and in making a detailed connection between single-particle and collective orientational motions. In addition, simulations of the aggregation kinetics in strongly polar fluids could shed light on the different time scales observed in recent experiments.[28] This might best be achieved through the application of computational methods devised for the study of energy landscapes.[39] These will be the topics of future studies.

ACKNOWLEDGMENT

P.D.D. is grateful to the Engineering and Physical Sciences Research Council (U.K.) for the provision of a studentship.

[1] P. I. C. Teixeira, J. M. Tavares, and M. M. Telo da Gama, J. Phys.: Condens. Matter **12**, R411 (2000).
[2] P. H. Hess and P. H. Parker, Jr., J. Appl. Polym. Sci. **10**, 1915 (1966).
[3] V. F. Puntes, K. M. Krishnan, and A. P. Alivisatos, Science **291**, 2115 (2001).
[4] K. Butter, P. H. H. Bomans, P. M. Frederik, G. J. Vroege, and A. P. Philipse, Nat. Mater. **2**, 88 (2003).
[5] K. Butter, P. H. Bomans, P. M. Frederik, G. J. Vroege, and A. P. Philipse, J. Phys.: Condens. Matter **15**, S1451 (2003).
[6] A. Zilman, T. Tlusty, and S. A. Safran, J. Phys.: Condens. Matter **15**, S57 (2003).
[7] T. Tlusty and S. A. Safran, Science **290**, 1328 (2000).
[8] P. Pincus, Science **290**, 1307 (2000).
[9] P. G. de Gennes and P. A. Pincus, Phys. Kondens. Mater. **11**, 189 (1970).
[10] P. C. Jordan, Mol. Phys. **25**, 961 (1973).
[11] M. A. Osipov, P. I. C. Teixeira, and M. M. Telo da Gama, Phys. Rev. E **54**, 2597 (1996).
[12] J. M. Tavares, M. M. Telo da Gama, and M. A. Osipov, Phys. Rev. E **56**, R6252 (1997).
[13] J. M. Tavares, J. J. Weis, and M. M. Telo da Gama, Phys. Rev. E **59**, 4388 (1999).
[14] J. J. Weis and D. Levesque, Phys. Rev. Lett. **71**, 2729 (1993).
[15] D. Levesque and J. J. Weis, Phys. Rev. E **49**, 5131 (1994).
[16] P. J. Camp and G. N. Patey, Phys. Rev. E **62**, 5403 (2000).
[17] P. J. Camp, J. C. Shelley, and G. N. Patey, Phys. Rev. Lett. **84**, 115 (2000).
[18] H. Mamiya, I. Nakatani, and T. Furubayashi, Phys. Rev. Lett. **84**, 6106 (2000).
[19] P. J. Camp, Phys. Rev. E **68**, 061506 (2003).
[20] W. D. Ristenpart, I. A. Aksay, and D. A. Saville, Phys. Rev. Lett. **90**, 128303 (2003).
[21] I. Varga, F. Kun, and K. F. Pál, Phys. Rev. E **69**, 030501 (2004).
[22] J.-J. Weis, Mol. Phys. **93**, 361 (1998).
[23] J. J. Weis, Mol. Phys. **100**, 579 (2002).
[24] J. J. Weis, J. M. Tavares, and M. M. Telo da Gama, J. Phys.: Condens. Matter **14**, 9171 (2002).
[25] J. M. Tavares, J. J. Weis, and M. M. Telo da Gama, Phys. Rev. E **65**, 061201 (2002).
[26] J. J. Weis, J. Phys.: Condens. Matter **15**, S1471 (2003).
[27] R. E. Rosensweig, *Ferrohydrodynamics* (Dover, New York, 1998).
[28] W. Wen, F. Kun, K. F. Pál, D. W. Zheng, and K. N. Tu, Phys. Rev. E **59**, R4758 (1999).
[29] V. V. Murashov, P. J. Camp, and G. N. Patey, J. Chem. Phys. **116**, 6731 (2002).
[30] T. A. Andrea, W. C. Swope, and H. C. Andersen, J. Chem. Phys. **79**, 4576 (1983).
[31] S. Fazekas, J. Kertész, and D. E. Wolf, Phys. Rev. E **68**, 041102 (2003).
[32] M. P. Allen and D. J. Tildesley, *Computer Simulation of Liquids* (Clarendon, Oxford, 1987).
[33] J.-P. Hansen and I. R. McDonald, *Theory of Simple Liquids* (Academic, London, 1986).
[34] B. J. Alder and T. E. Wainwright, Phys. Rev. A **1**, 18 (1970).
[35] M. M. Hurley and P. Harrowell, J. Chem. Phys. **105**, 10521 (1996).
[36] Of course, we could have obviated all of these problems by carrying out a longer MD simulation. To estimate the simulation time required, we fitted a single exponential function to the "tail" of $C_{\mu}^{xy}(t)$ for $\mu^*=2.75$ and $\rho^*=0.5$ in the region $t^*>3$. The decay constant was of the order of 0.01, which means that $C_{\mu}^{xy}(t)$ will have decayed to 1% of its initial value after a reduced time of about 500. To ensure good statistics one might need to perform a simulation at least 20 times longer in duration, which equates to a simulation consisting of 4×10^6 time steps. Unfortunately this is an order of magnitude longer than we can simulate with the current computational resources at our disposal.
[37] B. Bagchi and A. Chandra, Adv. Chem. Phys. **80**, 1 (1991).
[38] D. Kivelson and P. A. Madden, Mol. Phys. **30**, 1749 (1975).
[39] D. J. Wales, *Energy Landscapes: Applications to Clusters, Biomolecules and Glasses* (Cambridge University Press, Cambridge, 2004).